Composites Part B 140 (2018) 44–56

Contents lists available at ScienceDirect

Composites Part B

journal homepage: www.elsevier.com/locate/compositesb

Multifunctional graphene/POSS epoxy resin tailored for aircraft lightning strike protection

Marialuigia Raimondo[a,*], Liberata Guadagno[a,**], Vito Speranza[a], Leila Bonnaud[b], Philippe Dubois[b], Khalid Lafdi[c]

[a] Department of Industrial Engineering, University of Salerno, Via Giovanni Paolo II, 132, 84084 Fisciano, SA, Italy
[b] Laboratory of Polymeric and Composite Materials, Center of Innovation and Research in Materials & Polymers (CIRMAP), Materia Nova Research Center & University of Mons, 20 Place du Parc, 7000 Mons, Belgium
[c] University of Dayton, 300 College Park, Dayton, OH 45440, USA

ARTICLE INFO

Keywords:
Nano-structures
Thermosetting resins
Electrical properties
High-temperature properties
Surface analysis
Tunneling atomic force microscopy (TUNA)

ABSTRACT

This paper presents a first successful attempt to obtain a conductivity mapping at nanoscale level of a new multifunctional fire retardant graphene/polyhedral oligomeric silsesquioxane (POSS) epoxy resin using Tunneling Atomic Force Microscopy (TUNA) that is a very sensitive mode by which ultra-low currents ranging from 80 fA to 120 pA can be measured. The multifunctional material, specifically designed to meet structural aeronautical requirements, such as suitable thermal stability, fire resistance, mechanical performance and electrical conductivity, has proven to be a promising candidate in the field of aeronautic and aerospace composites. The results also highlight the great potentiality of TUNA technique to analyze conductive networks at nanodomain level. Through simultaneous topographic and current images acquisition, this technique enables a direct correlation of local topography with electrical properties of the nanofiller based samples. The intrinsic electrical conductivity of the manufactured polymeric systems allows TUNA measurements without using electrical conductive paint, which is usually employed for polymeric systems to ensure effective electrical contacts to the ground.

1. Introduction

Aeronautic structures differ from other structures as they need to meet two challenging criteria: high performance and lightweight. In this contest, graphene-based composites may play a game-changing impact in terms of performance and efficiency of future airframe. This is due to the electrical and other unique physical properties of graphene [1–9] that could allow smart integration into lightning strike protection, flame retardancy, impact resistance and others [10–24]. Engineered materials are required to resist degradation [25,26] during an unlikely event of fire in many critical applications such as skyscrapers, boats, or airplanes [27]. Materials used in aviation should be designed to inhibit, suppress, or delay the production of flames to prevent the spread of fire [28]. Epoxy based thermosetting nanocomposites are one of the most commonly used aeronautic materials in the aviation industry because of their excellent mechanical performance, chemical and electrical resistance, fire retardant properties and low shrinkage on curing [29–46] and they can be designed to be applied as multifunctional resins [10,28,43,47]. Materials of this kind offer *whopping* potential to impact future structural performance of advanced engineered composites with easy integration into current processing schemes [10] by reducing size, weight cost, power consumption and complexity while improving efficiency, safety and versatility. Successful strategies to reduce the flammability of epoxy resins [24,48,49], simultaneously increasing the electrical conductivity, are extremely important in the field of aeronautic and aerospace applications [28,37,43]. Currently, in the field of conductive lightweight resins, the material scientists have the possibility “to use” the advantages of the recent discoveries about nanofillers and nanotechnologies that can help to project materials working as multifunctional systems, in addition to the classical methods to protect the materials. Improvements in electrical percolation and mechanical performance have been obtained by a combined action due to a nice balance between the exfoliation degree and the chemistry of graphene edges which promotes the interfacial interaction between polymer and carbon layers [37]. Current chemical technology aimed at increasing the flame resistance of polymeric and composite materials and providing, at the same time, new tools for chemical and materials research is based on cage-like POSS

* Corresponding author.
** Corresponding author.
E-mail addresses: mraimondo@unisa.it (M. Raimondo), lguadagno@unisa.it (L. Guadagno).

https://doi.org/10.1016/j.compositesb.2017.12.015
Received 17 September 2017; Received in revised form 7 December 2017; Accepted 15 December 2017
Available online 16 December 2017
1359-8368/

nanostructured molecules composed of silicon and oxygen [28,43] with the empirical formula $RSiO_{1.5}$, where R attached to the corners of the cage may be a hydrogen atom or an organic functional group, e.g., alkyl, alkylene, acrylate, hydroxyl or epoxide unit [50–54]. The organic pendent groups can be designed to achieve the desired affinity with the host polymeric matrix [55]. Lightning strike to aircraft, where there is a direct contact between the aircraft surface and the lightning arc, represents a possible safety hazard. Lightning is a discharge of electricity that occurs in the atmosphere and can be thought of as a high-current — about 20,000 A — electric spark associated with thunderstorms. The effects of a lightning strike on aircraft are classified into two main categories: while direct effects are associated with physical damages occurring at the attachment point and in equipment, the indirect effects concern the interferences due to the electromagnetic coupling with the systems and the cabling [56].

Actually, several lightning strike protection (LSP) strategies have been adopted for composite aircrafts [57]. The goal of lightning protection is to prevent accidents and increase the reliability of aircraft. Aeroplanes have metal shells that prevent passengers being affected by lightning strikes. One of the main drawbacks arising from the transition from electrically conductive metals to insulating or semi-conducting composites is the higher vulnerability of the aircraft to lightning strike damage. Aircraft structures are being redesigned to use fiber-reinforced composites mainly due to their high specific stiffness and strength [58]. It is well known that carbon fiber composites are used extensively in aircraft applications such as fuselages, leading edges and wing surfaces because the carbon fibre is light and strong thus allowing for aircraft to consume less fuel. Unfortunately, the fiber reinforced polymer (FRP) composites are unable to conduct the high electrical currents and electromagnetic forces sufficiently to prevent structural damage. When lightning strikes or lightning currents pass through these composite structures, the result can be embrittlement, delamination, and/or structural failure [59]. There is a need for a lightning strike protection (LSP) solution that enables lightning currents and electromagnetic interference (EMI) forces to flow through the aircraft's protection system harmlessly, and exit at the other end towards the ground. The most severe damage usually occurs at the entrance or exit of lightning strikes where the energy density is highest. Major aerospace companies are dealing with the issue of LSP by investigating methods in order to enhance LSP protection on composite parts so that damages are reduced or eliminated. The current protection approach consists of bonding a metal mesh to the surface of the composite structure, but this weight increase negatively impacts on the fuel efficiency and as a consequence on the environmental pollution. The main challenge to replace the current metallic mesh technology is to find a material with a higher conductivity/density ratio or a solution that makes use of lightning physics to avoid damage to the aircraft. In this regard, recently, there is an enormous increase of research and development activities on graphene-reinforced polymers [57] and many research projects are funded with the goal of exploiting the wonderful graphene's electricity-conducting properties that can be incorporated into the carbon fibre. It is known that the addition of small quantities of graphene materials can simultaneously provide significant improvements in strength, toughness, electrical and thermal conductivity, and chemical inertness to a number of polymers [5–8,57,60,61].

Hence, the exploitation of a new generation of aerospace nano-reinforced composite systems with additional functionalities which combine enhanced mechanical and thermal properties with flame retardant abilities without compromising structural integrity represents a peremptory aspect in the current aerospace technology [28,36–43,62]. Furthermore, in order to dissipate lightning currents without employing conductive metal fibers or metal screens, the electrical conductivity of structural parts such as aircraft fuselages has to reach 1–10 $S\,m^{-1}$ [42,46]. Surface science and nanotechnology have both grown rapidly in the past decades, and are still among the most active fields of research. Simultaneously, the semiconductor technology was significantly enhanced by account of the implementation of novel approach which rely on the application of surface properties.

Besides, the need for electrical characterization of surfaces on the nanometer scale in order to improve local conductivity measurements has led quickly to a variety of scanning probe microscopy based techniques. For this type of measurements, usually, two different setups performed in contact mode are used; conductive atomic force microscope (C-AFM) [63–66] and tunneling AFM (TUNA) [67,68] depending on the range of currents involved. The first is used to measure current in the range of sub-nA to μA (in particular, higher currents can be measured ranging from 1 pA to 1 μA), the latter for the range between sub-pA to nA (in particular, ultra-low currents (< 1 pA) ranging from 80 fA to 120 pA can be measured). In this work, TUNA which utilizes a conductive probe during the measurement process was used.

Our recent research focused on developing high performance polymer nanocomposites, with the benefit of carboxylated partially exfoliated graphite (CpEG) and flame retardant glycidyl polyhedral oligomeric silsesquioxane (GPOSS) nanoparticles, to achieve a novel multifunctional epoxy resin. This paper presents the first successful attempt to obtain a conductivity mapping of a new multifunctional epoxy resin by TUNA. This novel technology allows to simultaneously map the topography and conductivity of advanced material by applying controlled, low forces on the tip during imaging, which allows a direct comparison between the morphology and the electrical properties at the nanoscale [67,69–72].

In this technique, that uses a conductive AFM probe in contact mode, the sensor signal is the electric current between the AFM tip and the conductive sample for an applied DC bias. This non-contact technique helps in carrying out various non-destructive measurements on electrical conductive nanoparticles to obtain point measurement scan of the sample topography and its corresponding electrical data. On the basis of our knowledge, there are currently few works that report a characterization based on this new technique. The multifunctional system has been specially designed so as to meet specific aeronautical requirements through tailored properties by identifying the best strategy for improving its thermal, fire resistance and electrical conductivity. In particular, this paper focus on electrical characterization at nanoscale level using Tunneling AFM (TUNA) and flammability behavior of a new multifunctional nanocomposite. The increase of limiting oxygen index (LOI) value, the decrease of the peak of heat release rate (PHRR) value, observed when GPOSS is used, and the increase of the time of ignition due to the inclusion of CpEG in epoxy systems, together with the high electrical and mechanical properties and the good thermostability imparted by self-assembly blocks of CpEG nanofiller, support the possibility of creating a true multifunctional composite.

2. Experimental and methods

2.1. Materials and epoxy specimens manufacture

The two dimensional (2D) predominant shape CpEG nanoparticles were prepared starting from high surface area of natural low density flake graphite (FG) (Asbury graphite grade 3759, Asbury Carbons, NJ) that is characterized by the following parameters: Carbon purity % = 98.6, Size 1" × 8 mesh, Bulk Density (g/100 mL) = 17.80, Sulfur (%) = 0.056 and Resistivity (Ω cm) = 0.0316. The elemental analysis of the CpEG graphitic sample highlighted an oxygen content of 8.5 wt %. [37]. The sample CpEG was prepared as follows: a mixture containing nitric and sulfuric acid and natural graphite was used. After 24 h of reaction, intercalation within graphene sheets took place to form intercalated graphite compound (IG). Then the mixture was filtered, washed with water, and dried in an oven at low temperatures. The intercalated graphite compound was subjected to sudden heat treatment temperature of 900 °C and rapid expansion then occurred. The expansion ratio was as high as 300 times. Changes in the degree of exfoliation was obtained by varying the resident time in the fluidized

bed as the time increases, the trapped intercalate and/or gases would have a second the chance to escape causing further expansion and exfoliation. In this work, the CpEG used is characterized by a degree of exfoliated phase of 60% and a number of 29 stacked monolayer sheets [37] that means an average thickness about 0.980 Å assuming the thickness of single graphene layer to be about 0.34 nm [73]. CpEG sample contains a high concentration of carboxylated groups at the edge of graphene layers, with an amount of about 10 wt% [37]. GPOSS molecule is functionalized with oxirane groups.

The epoxy matrix T20B was prepared by mixing an epoxy precursor, tetraglycidyl methylene dianiline (TGMDA) (*Epoxy equivalent weight* EEW 117–133 g/eq) with an epoxy reactive diluent 1–4 Butanediol diglycidyl ether (BDE) at a concentration of 80%:20% (by wt), respectively. The unfilled epoxy resin T20BD was obtained after addition of the 4,4′-diaminodiphenyl sulfone (DDS) curing agent at a stoichiometric concentration with respect to all the epoxy rings (TGMDA and BDE). The viscous liquid GPOSS was solubilized at 5 wt% in the epoxy mixture T20B using two steps: ultrasonication at 90 °C (Hielscher model UP200S-24 KHz high power ultrasonic probe) and magnetic stirring in oil bath at 120 °C for 1 h. The chosen procedure allows a good level of dissolution into the initial liquid epoxy mixture [28,43]. Then, the sample T20BD + 5%GPOSS was obtained by adding DDS at a stoichiometric concentration with respect to all the epoxy rings (TGMDA, BDE and GPOSS). In our previous work [28], the incorporation of 5 wt% of GPOSS into epoxy resin has been found to be beneficial for improving its flame retardancy. Data on the dispersion of GPOSS within the epoxy mixture T20B showed that the structure of the POSS compound plays an important role on the its dissolution/dispersion into the matrix. The effective dissolution of GPOSS in the initial liquid epoxy mixture is most probably due to the structure of GPOSS that is fully epoxidized with glycidyl groups which makes compatible the POSS molecule with epoxy precursors and reactive diluent. In addition, its structure allows the reaction and inclusion into the T20BD network formation during the curing cycle. This could explain the better behavior of GPOSS compared to the other analyzed POSS. Finally, the multifunctional nanocomposite T20BD + 5%GPOSS + 1.8%CpEG was obtained by incorporating CpEG nanofiller at 1.8 wt% into the T20B + 5%GPOSS mixture through an ultrasonication for 20 min and, then, by adding DDS. It is worth noting that the multifunctional epoxy resin T20BD + 5%GPOSS + 1.8%CpEG has been appropriately designed taking into account the best strategy aimed at finely balancing the thermal, fire resistance, mechanical performance and electrical conductivity of an epoxy resin for aeronautic application [28,37,47]. In this regard, it was possible to fulfil this ambitious goal through a nice combination of the conductive T20BD + 1.8%CpEG and the flame retardant T20BD + 5%GPOSS nanocomposites in light of the remarkable results obtained for these two formulations [28,37,47]. In particular, the nanofilled epoxy resin T20BD + 1.8%CpEG showed enhanced mechanical and electrical properties (the DC conductivity at the loading of 1.8% wt for CpEG has reached the value of about 0.096 S m^{-1}) due to a self-assembly structure in the epoxy matrix using edge-carboxylated layers approach that favors the electrical percolative paths also increasing the nanofiller/epoxy matrix interaction thus determining a relevant reinforcement in the storage modulus [37].

TGMDA, BDE, DDS were purchased from Sigma-Aldrich, and GPOSS compound from Hybrid Plastics Company. All the mixtures were cured by two-stage curing cycles: a first isothermal stage was carried out at the lower temperature of 125 °C for 1 h and, then, a second isothermal stage at higher temperatures up to 200 °C for 3 h. Fig. 1 shows the chemical structures of compounds used for the epoxy-amine composites and a visual observation of the CpEG. Scheme shown in Fig. 2 summarizes the preparation procedure steps of the multifunctional epoxy nanocomposite T20BD + 5%GPOSS + 1.8%CpEG.

The photographs of the tested epoxy specimens, appropriately prepared with different geometries depending on the type of test performed, after the curing and extraction from the molds are shown in Fig. 3.

2.2. Methods

2.2.1. Dynamic mechanical analysis (DMA)

Dynamic mechanical properties of the multifunctional nanocomposite T20BD + 5%GPOSS + 1.8%CpEG were performed with a dynamic mechanical thermo-analyzer (Tritec 2000 DMA -Triton Technology). Solid samples with dimensions 2 × 10 × 35 mm^3 were tested by applying a variable flexural deformation in three points bending mode. The displacement amplitude was set to 0.03 mm, whereas the measurements were performed at the frequency of 1 Hz. The range of temperature was from −90 °C to 315 °C at the scanning rate of 3 °C/min.

2.2.2. Thermogravimetric analysis (TGA)

Thermogravimetric analysis (TGA) was carried out using a Mettler TGA/SDTA 851 thermobalance. The samples were heated from 25 °C to 900 °C at a 10 °C/min heating rate under both nitrogen and air flows. The weight loss was recorded as a function of temperature.

2.2.3. Fire resistance

Fire resistance of the solidified epoxy samples was characterized by limiting oxygen index (LOI) measurement and mass loss calorimetry in order to obtain peak of heat release rate (PHRR) and ignition time (t_i) data. The peak of heat release rate (PHRR) represents the maximum amount of heat released by the material during the combustion process and frequently occurs shortly after the ignition. The ignition time is defined as the time a combustible material can support, when exposed to a constant radiant heat flux, before initiating ignition and be subjected to combustion with continuous flame. It can be used as a simple measure of the material's resistance to fire. The ignition time depends on several factors, namely the oxygen availability, the temperature, and the chemical and thermo-physical properties of the polymer matrix and the reinforcement [74].

Experimental conditions for LOI tests: barrels of 80 × 10 × 3 mm^3 are fixed in a vertical position and their top is inflamed with a burner. LOI, the minimum concentration of oxygen in a nitrogen/oxygen mixture required to just support the sample combustion, was measured following standard ASTM 2863.

Experimental conditions for Mass loss calorimeter: plates of 100 × 100 × 3 mm^3 are exposed to a radiant cone (50 kW/m^2) using a forced ignition. The heat of combustion released was measured using a thermopile according to standard ISO 13927.

2.2.4. Scanning electron microscopy (SEM) analysis

Micrographs of the epoxy nanocomposites were obtained using Scanning Electron Microscope-SEM (mod. LEO 1525, Carl Zeiss SMT AG, Oberkochen, Germany). All samples were placed on a carbon tab previously stuck to an aluminum stub (Agar Scientific, Stansted, UK) and were covered with a 250 Å-thick gold film using a sputter coater (Agar mod. 108 A). Nanofilled sample sections were cut from solid samples by a sledge microtome. These slices were etched before the observation by SEM. The etching reagent was prepared by stirring 1.0 g potassium permanganate in a solution mixture of 95 mL sulfuric acid (95–97%) and 48 mL orthophosphoric acid (85%). The filled resins were immersed into the fresh etching reagent at room temperature and held under agitation for 36 h. Subsequent washings were done using a cold mixture of two parts by volume of concentrated sulfuric acid and seven parts of water. Afterward the samples were washed again with 30% aqueous hydrogen peroxide to remove any manganese dioxide. The samples were finally washed with distilled water and kept under vacuum for 5 days before being subjected to morphological analysis.

2.2.5. Transmission electron microscopy (TEM) analysis

Transmission electron microscopy (TEM) analysis was performed

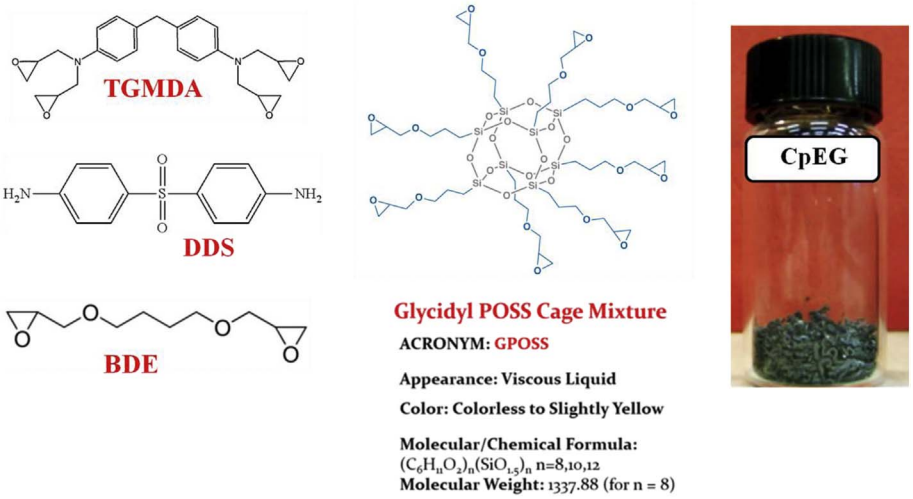

Fig. 1. Chemical structures of compounds used for the epoxy-amine composites and a visual observation of the CpEG.

with a Philips CM100 apparatus using an acceleration voltage of 100 Kv. Some of the nanocomposites sections were cut from the solid samples by a sledge microtome. The sample slices were etched before the morphological observation.

2.2.6. Atomic force microscopy (AFM) and Tunneling Atomic Force Microscopy (TUNA) analysis

Atomic force microscope (AFM) images were acquired in an ambient atmosphere (30%–40% humidity) with a Dimension 3100 coupled with a Bruker NanoScope V multimode AFM (Digital Instruments, Santa Barbara, CA) controller operating in tapping mode (TM-AFM) or in tunneling current mode (TUNA-AFM), using microfabricated silicon tips/cantilevers. The AFM acquisitions were kept using the tapping mode in order to minimize the interaction with the sample surface. For tapping mode, commercial probe tips with nominal spring constants of 20–100 N m^{-1}, resonance frequencies in the range of 200–400 kHz, and tip radius of 5–10 nm were used. The TUNA-AFM measurements were performed using platinum-coated probes with nominal spring constants of 35 N m^{-1} and electrically conductive tip of 20 nm. TUNA -AFM operates in contact mode. TUNA works similarly to C-AFM but with higher current sensitivity. The sensor signal is the electric current between the afm tip and the conductive sample for an applied DC bias. In feedback mode, the output signal is the DC bias, adjusted to maintain the electric current setpoint. The following values of the TUNA control parameters are used: DC sample bias ranged from 1 V to 2 V taking into account that bias limit is 12 V, current sensitivity was 1 nA/V, current range was 200 nA, samples/lines: determines the number of data points or pixels in X and Y (256), scan rate: controls the rate at which the cantilever scans across the sample area (0.9–1.5 Hz s^{-1}). In order to obtain repeatable results, different regions of the specimens were scanned. By adopting TUNA-AFM is possible to perform electrical characterization at nanoscale level without grounding the samples. The images were analyzed using the Bruker software Nanoscope Analysis 1.80 (Build R1.126200). Tunneling atomic force microscopy which has been given the official designation 'TUNA' by the equipment manufacturers (Bruker) is a highly sensitive technique by which ultra-low currents (< 1 pA) ranging from 80 fA to 120 pA can be measured [68]. TUNA allows a tunneling current to be obtained from a nanosharp tip attached to a cantilever while simultaneously moving the tip across the sample surface to measure topographical data. In contrast to standard STM which requires sample surfaces to be smooth on the nanometer scale, TUNA can investigate surfaces with an r.m.s. roughness of several microns. Moreover, the surface can be studied over scan areas up to hundreds of square microns, allowing a wider picture of the overall morphology to be obtained. Furthermore, unlike the constant-current mode of STM, the physical tracking of TUNA means that the height data collected from the deflection of the cantilever avoids possible artefacts introduced by variations in the conductivity of the sample surface.

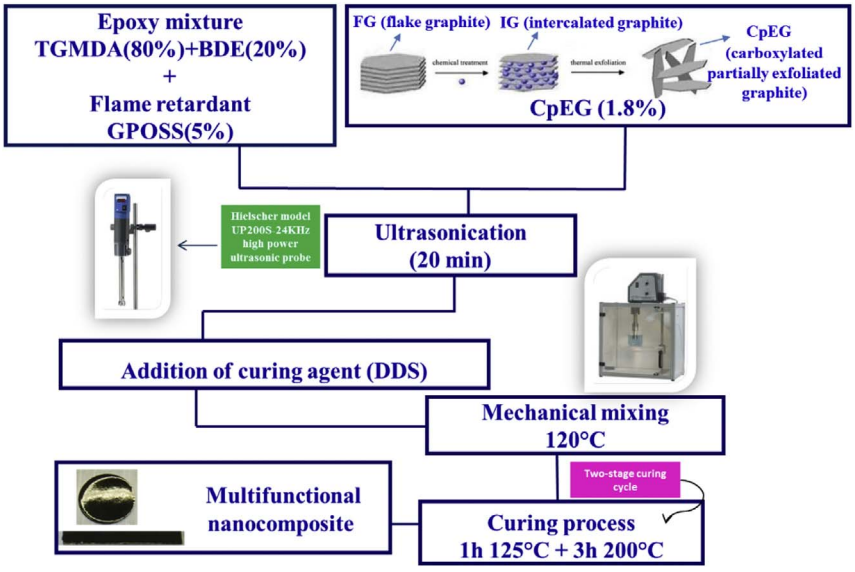

Fig. 2. Scheme of the preparation procedure of the multifunctional epoxy nanocomposite T20BD + 5%GPOSS + 1.8%CpEG.

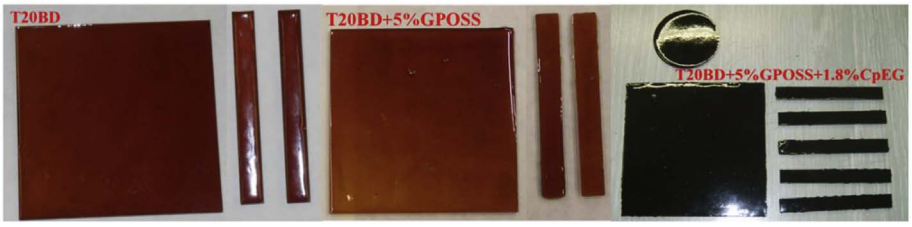

Fig. 3. Photographs of the tested epoxy specimens, appropriately prepared with different geometries depending on the type of test performed, after the curing and extraction from the molds.

Another major advantage of TUNA is that it has very high current sensitivity with a noise level of 50 fA [75].

2.2.6.1. Working principle of Tunneling Atomic Force Microscopy (TUNA). Besides conventional AFM's scanner and cantilever detection technique, the TUNA setup employs a conductive AFM probe, an external voltage source needed to apply a potential difference between the tip and the sample holder, and a current amplifier used to convert the (analogical) current signal into (digital) voltages that can be read by the computer [76]. In particular, in our experiments, TUNA operated with a cantilever holder and an epoxy nanofilled sample (containing conductive graphene nanoparticles) electrically connected to an external voltage source (see Fig. 4).

In TUNA experiments, the sample is usually fixed on the sample holder using a conductive tape or paste, being silver paints the most widespread. In this regard, it is worth noting that the samples investigated in this work have not undergone any prior treatment with silver paint that is usually used to create electrical contacts to the ground. The principle of the TUNA mode (see Fig. 4), based on an ohmic contact formed between the conductive AFM tip and the sample surface, is the same as C-AFM, by which simultaneous topographic imaging and current imaging can be collected. For the electrical measurements of the samples, just like contact mode AFM, the z-feedback loop uses the dc cantilever deflection as a feedback signal to maintain a constant force between the tip and the sample to generate the topography image [77]. In fact, during scanning, a constant DC bias voltage is applied between the tip and the sample and thus the resulting current through the sample is measured with a current amplifier in order to obtain the desired electrical information. TUNA is performed by adding a specialized module to the AFM head and mounting the cantilever in a holder with a current output. The module contains a test connector for calibration and a sensor input connector for connection with the cantilever holder. During operation, the tip-sample force (deflection setpoint) and DC bias voltage are then adjusted to optimize contrast between low and high conductivity regions on the surface [78]. In this work, the TUNA application module was operated in imaging mode, where images of the electrical current are obtained.

The amplification is especially important for samples with high resistance or even isolating behavior, where the measured currents can be as low as several femto-to picoamperes. The TUNA technique bears a striking resemblance to Scanning Tunneling Microscopy (STM) using similar technical solutions for the current signal acquisition. However, there is a fundamental difference in the operational principle. In contrast to STM, the TUNA measures the current signal completely independent from the topography which is simultaneously recorded via the cantilever deflection. In order to obtain a potential drop and current across the sample, the external bias is applied to the sample. It is also worth to notice that the contact to the sample should be preferentially ohmic, otherwise the influence of the additional barrier has to be considered carefully. The commonly used range of the applied voltage is ± 10 V. The application of higher voltages is possible using external voltage sources, though additional circuit protection should be implemented.

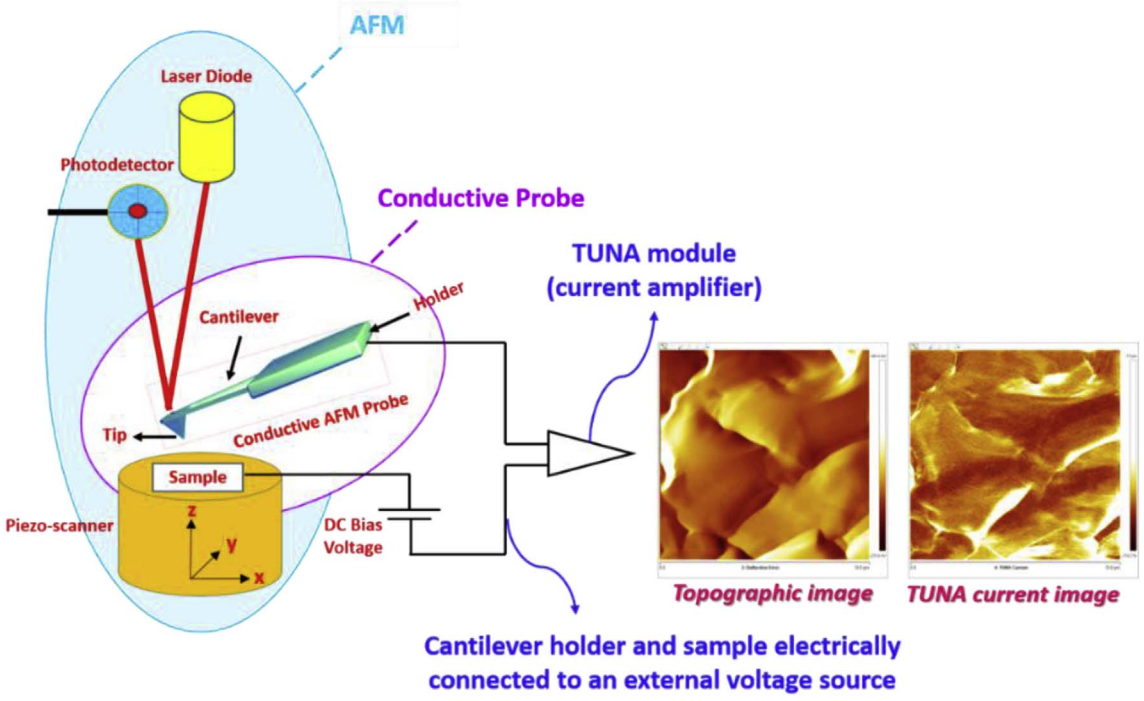

Fig. 4. Experimental setup of the Tunneling AFM (TUNA).

Table 1
LOI and PHRR values of the tested epoxy samples.

SAMPLE	LOI ($\%O_2$) (% ± 1)	PHRR (kW/m^2)	t_i (% ± 2) (s)
T20BD	27	540 ± 81	40
T20BD + 5%GPOSS	33	327 ± 49	42
T20BD + 1.8%CpEG	25	882 ± 110	42
T20BD + 5%GPOSS + 1.8%CpEG	30	560 ± 82	62

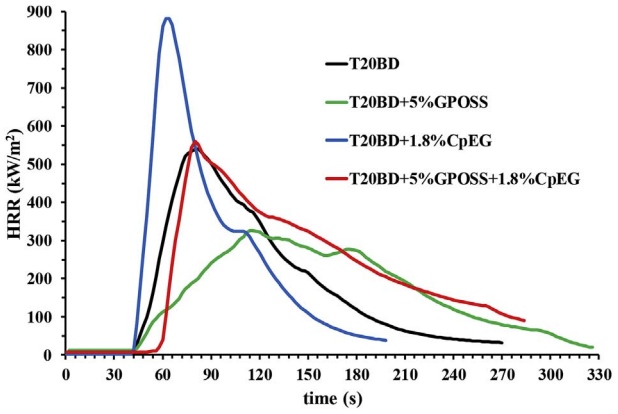

Fig. 5. HRR of the unfilled and nanofilled epoxy formulations.

3. Results and discussion

3.1. Fire behavior of epoxy formulations

Table 1 gathers the limiting oxygen index (LOI), the values of the peak of heat release rate (PHRR) and the ignition time (t_i); errors based on the maximum deviation from single averaged values are provided.

In the following, the HRR versus time curves for the unfilled and nanofilled epoxy samples are also shown in Fig. 5. It is clearly evident that, in nanofilled multifunctional composites, GPOSS acts as flame retardant as already found in literature [28,43]. In particular, GPOSS 5 wt% mixed with the unfilled epoxy matrix determines an enhancement in the LOI value of about 23% and a decrease in the PHRR value of about 40%, whereas no significant difference is observed in the values of the ignition time.

The beneficial effect of GPOSS on the flame behavior of epoxy formulations has been ascribed to the structure of GPOSS which is fully epoxidized with glycidyl groups making compatible GPOSS molecules with epoxy precursor and reactive diluent. The dispersion of CpEG 1.8 wt% in the epoxy mixture T20BD worsens the flame behavior of the filled formulation as evidenced by the strong increase in the PHRR (~63% with respect to T20BD) and the decrease in LOI (~7% with respect to T20BD). The presence of GPOSS in combination with CpEG significantly improves the flame behavior as evidenced by the decrease in PHRR value (37%) and the increase in LOI value (20%) with respect to the nanofilled formulation. Furthermore, an increase of about 55% in the ignition time is detected for the sample T20BD + 5%GPOSS + 1.8%CpEG which exhibits the best behavior with respect to all the analyzed samples. It is worth noting that the unfilled epoxy formulation T20BD (without GPOSS) chosen to formulate the nanocomposites is already characterized by a lower value in PHRR (540) and higher value in the LOI value with respect to epoxy formulations already studied in literature [79]. Hence, the possibility to obtain nanofilled resins with all the advantages related to the presence of graphene-based nanoparticles, without deterioration in the flame behavior, opens new interesting prospectives of industrial applicability in the field of structural/functional materials. Concerning the interest in the applicability, it is worth noting that the multifunctional fire-retardant epoxy nanocomposite T20BD + 5%GPOSS + 1.8%CpEG shows the highest value of ignition time (62 s) compared to all the epoxy formulations analyzed in this work and previous publications [28,43]. Furthermore, the presence of 1.8 wt% of CpEG in combination with GPOSS allows to obtain a material exhibiting the value in the electrical conductivity of 1.33 S m^{-1} [43] with respect to the value of 8.00×10^{-13} S m^{-1} of the unfilled formulation T20BD [36,41,42,80–82] and the value of 9.60×10^{-2} S m^{-1} of T20BD + 1.8%CpEG [37]. The high electrical conductivity shown by multifunctional nanocomposite T20BD + 5%GPOSS + 1.8%CpEG is really remarkable if one considers that, in order to efficiently dissipate lightning currents without employing conductive metal fibers or metal screens, the electrical conductivity of structural parts such as aircraft fuselages has to reach values at least between 1 and 10 S m^{-1} [42,46].

3.2. Thermogravimetric analysis (TGA)

The thermal behavior of the formulated epoxy resins was studied in both oxidative and non-oxidative conditions by using thermogravimetric analysis (TGA). Fig. 6 shows the TGA curves in air and in inert (N_2) atmosphere of the unfilled resin T20BD and multifunctional nanocomposite T20BD + 5% GPOSS + 1.8%CpEG.

In air, within the experimental temperature range, a two-step thermal degradation process can be observed for the two samples, suggesting that the inclusion of GPOSS and CpEG nanoparticles in the matrix does not significantly modify the degradation mechanism of the formulation. As expected, no residual yield was obtained at 900 °C for the unfilled resin T20BD. The residual yield for the resin containing GPOSS and CpEG nanoparticles is about 6 wt%, value very close to the theoretical values of the residual silica contents in the resin. TGA curves in air highlight that, compared with the unfilled sample T20BD, the

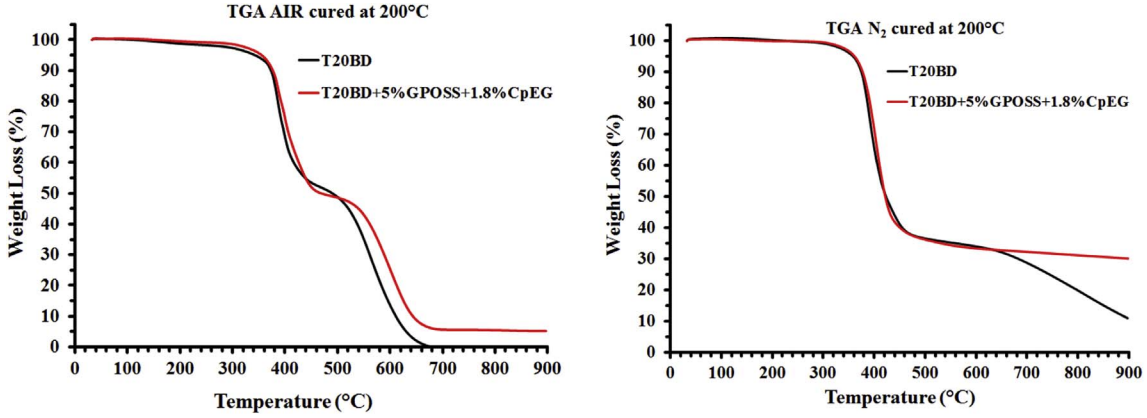

Fig. 6. TGA curves of the unfilled resin T20BD and multifunctional nanocomposite T20BD + 5% GPOSS + 1.8%CpEG.

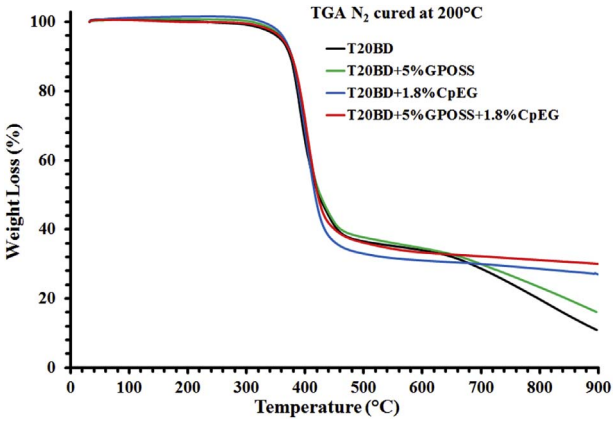

Fig. 7. TGA curves in nitrogen of T20BD, T20BD + 5%GPOSS, T20BD + 1.8%CpEG and T20BD + 5%GPOSS + 1.8%CpEG samples.

multifunctional epoxy resin T20BD + 5%GPOSS + 1.8%CpEG shows a slight increase in the thermal stability related to the first stage of the degradation process and a substantial increase in the second stage which is even more significant in nitrogen. Two distinct and well-separated turns also for TGA curves in nitrogen are observed. The beginning of the first step is in the same temperature range for both the samples, whereas the second step is much slower in N_2 with respect to the degradation in air. A very interesting result is the different mass loss at the end of the first stage; it is between 60 and 70% in nitrogen and 45–53% in air, this effect is not influenced by the presence of nanofiller; whereas the second step is strongly affected by the presence of the CpEG nanofiller. A comparison between the degradation behavior in N_2 for all the analyzed sample is shown in Fig. 7.

The detected TGA curves highlight that CpEG based nanoparticles effectively act in the stabilization of the formulation during the degradation stage. A similar effect, although to a much smaller extent, is played by the dispersion of GPOSS nanocages in the matrix (green curve). The higher thermal stability detected for the multifunctional T20BD + 5%GPOSS + 1.8%CpEG with respect to all the analyzed formulations is most likely due a synergistic action of GPOSS and CpEG, even considering that, the high thermal conductivity of graphene sheets might facilitate heat dissipation within nanocomposites and consequently improved the thermal stability of the entire sample [62]. The different trend of the thermogravimetric curves in air and inert (N_2) atmosphere (see Fig. 6) is a clear evidence that the beginning of the first stage is due to degradation processes which do not involve oxygen (dehydration, random scission etc), whereas the second step is strongly dependent on the oxygen availability. The longer thermal decomposition in nitrogen, during the second stage, has been already found in literature [28,37,83–85]. It has been ascribed to decomposition and release of various fragments over a wider temperature range with respect to the second stage in air [83]. In particular, in air atmosphere the fragments are oxidized whilst the resin is decomposing (II stage). The first stage leads to production of a carbonaceous residue, which is stable at lower temperatures, but is oxidized at higher temperatures [85]. The char oxidation stage in air occurs in the temperature range of 500°C–680 °C for the sample T20BD and 540°C-700 °C for the sample T20BD + 5%GPOSS + 1.8%CpEG, causing mass losses of 47% and 39% for the samples T20BD and T20BD + 5%GPOSS + 1.8%CpEG respectively. It is worth noting that no mass loss is observed in nitrogen atmosphere for the sample T20BD + 5%GPOSS + 1.8%CpEG which highlights a char residue of about 30% even at the temperature of 900 °C. The results of a previous paper highlighted the effect of exfoliation degree and the role of edge-carboxylated graphite layers of CpEG in giving self-assembled structures embedded in the polymeric matrix. The graphene-based layers inside the matrix form building blocks of complex systems that outperform the host matrix T20BD [37]. It is very likely that this particular arrangement strongly limits the oxidation mechanisms most of all in inert atmosphere.

It is worth noting that the neat T20BD system exhibits a continual crispy char relevant of quite a good thermostability of the neat system. Nevertheless, no intumescence is observed for this system without GPOSS. For the system containing GPOSS particles, intumescent char is obtained highlighting that the incorporation of POSS significantly enhances the thermostability of the char [28]. The inclusion of CpEG is found to decrease and even suppress the intumescence effect brought by GPOSS particles, confirming thermal conduction takes place all over the material limiting the flame retardancy of the material. This behavior is most likely due to a good transport of thermal energy in carbonaceous nanostructures ascribable to phonon conduction mechanism which is more effective through carbonaceous nanostructures characterized by two-dimensional flat shape [62,86,87]. However, the residue of the CpEG based systems is found to exhibit a more compact aspect stressing the ability of CpEG to also promote char formation. In summary, CpEG appear to act following two antagonist ways.

3.3. Dynamic mechanical analysis (DMA)

Dynamical mechanical data provide useful information on the relaxation processes that become operative in the polymer in a temperature range depending on the examined system. Fig. 8 shows the storage modulus (see on the left) and loss factor (tanδ) (see on the right) of T20BD and T20BD + 5%GPOSS + 1.8%CpEG epoxy formulations. As expected, a decrease in the storage modulus in the temperature range −90 °C to about 250 °C is observed for both samples; although the detected values are suitable in the usual operational temperature range of structural materials [47]. Considering that the only CpEG on the storage modulus of epoxy resins tends to increase the values [36], the lower value in the storage modulus of the sample T20BD + 5% GPOSS + 1.8%CpEG is most likely due to the role of the plasticizer effect of

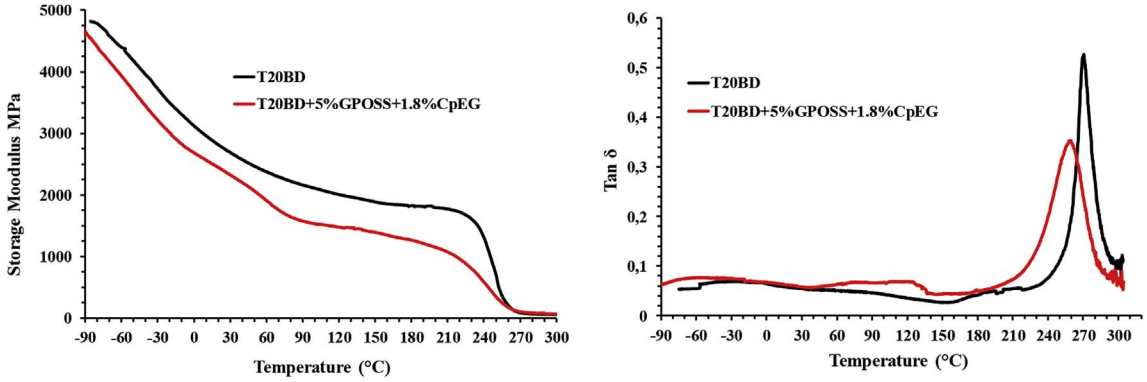

Fig. 8. Storage Modulus (see on the left) and Loss factor (tanδ) (see on the right) of the T20BD and T20BD + 5%GPOSS + 1.8%CpEG epoxy formulations.

POSS domains [88]. In the epoxy network, the influence of the POSS cage which is considered as an interacting crosslink and a plasticizer with high free volume. Interestingly, the epoxy reacted with POSS has fewer epoxide ring, namely a higher epoxy equivalent weight (EEW), resulting in a lower crosslinking density. The decrease of the epoxy crosslink density leads to easiest chain motion and decreases Tg. In our work, the plasticizing effect introduced by POSS cage seems to be more important and would explain the dynamic mechanical properties of the T20BD + 5% GPOSS + 1.8%CpEG sample. The loss factor (tan δ) is a measurement of damping property, which is the relation between the elastic energy stored and the energy dissipated per cycle of vibration. The glass transition temperature (Tg) for the T20BD + 5% GPOSS + 1.8%CpEG sample decreases with respect to the epoxy formulation T20BD. In fact, for the T20BD + 5% GPOSS + 1.8%CpEG nanocomposite, differences in the location and magnitude of the transition peak are visible. The decrease observed in the temperature of the main peak of tan δ curve is most likely due to a lower density of the resin network and the plasticizer effect of POSS domains. In any case, the Tg values for all two tested formulations are in the range between 260 and 270 °C, which are suitable for a very wide range of structural applications.

3.4. Morphological analysis

The morphological characterization of CpEG nanofiller and CpEG based nanocomposites carried out by means AFM, TEM and SEM techniques is shown in Fig. 9. We can clearly observe a very interesting morphological feature of the CpEG nanofiller in the SEM images (showed at three different magnifications:1 mm, 100 μm, and 20 μm) and the fracture surface of the T20BD + 1.8%CpEG sample in AFM-3D and TEM images. SEM images of the CpEG nanofiller shows a cellular structure that is associated with a large expansion (in this work the expansion rate was as high as 300 times) that results in a fluffy morphology. It was found that, most commonly, the graphite prior to exfoliation is in the form of flakes, which have the graphite c-axis perpendicular to the plane of the flake [73]. Because of the large expansion along the c-axis, the exfoliated flake becomes long in the direction that corresponds to the c-axis of the flake prior to exfoliation. As a consequence, the CpEG made from a graphite flake looks like a worm, and is known as a worm [73], as it is clearly visible especially in the SEM image at low magnification (1 mm) and also in the image of CpEG (a part of a worm) at a high magnification (100 μm). In the AFM-3D and TEM images of T20BD + 1.8%CpEG sample, self-assembly of carboxylated graphene sheets and thin graphite blocks (with thickness ranging from 1 nm to about 16 nm and diameters ranging from sub-micrometer to hundreds of μm) is observable and it seems to lead to extended architectures assembled along the sample. The distance between graphitic stacks is approximatively between 5 and 10 nm [37]. The CpEG dispersion in the polymeric matrix both in presence and absence of GPOSS was analyzed by SEM investigation on etched samples. The etching procedure consumes part of the surface layers of the epoxy matrix making possible a clearer observation of the dispersion state of the nanofiller, as already experienced with resins filled with carbon based nanofiller [36,37,47]. Fig. 10 shows SEM images at different magnifications of the fracture surface of the two epoxy-based composites filled at loading rate of 1.8 wt% of CpEG with GPOSS and in absence of GPOSS. The observation of the image in Fig. 10 highlights that, in both cases, the nanofillers seem uniformly dispersed in the polymeric matrix, but in the case of the matrix containing GPOSS, the CpEG nanoparticles seem better dispersed in the resin. This better distribution could be due to the decrease in the viscosity of the matrix containing GPOSS which also allows a better nanofiller dispersion making the phase at higher mobility well dispersed in the composite. GPOSS's ability to improve the dispersion of carbonaceous nanoparticles has also been detected for the epoxy resin nanofilled with multiwalled carbon nanotubes, as

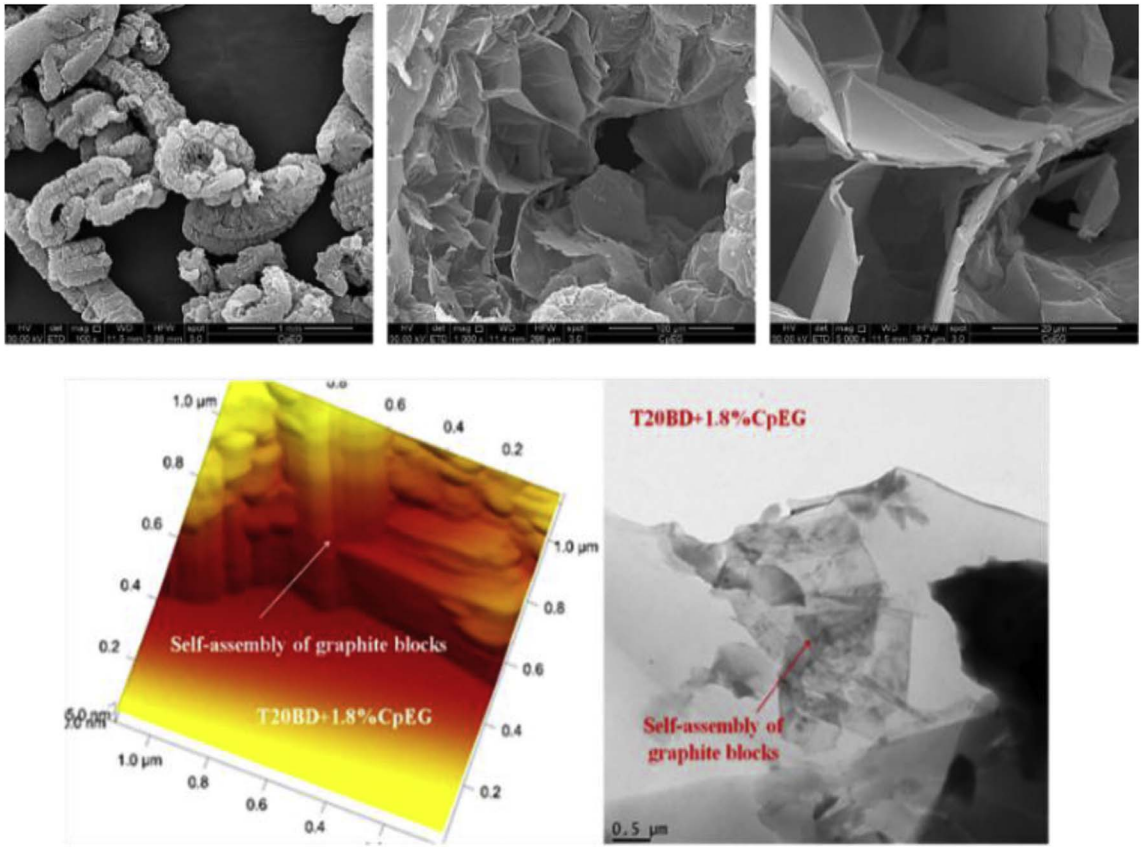

Fig. 9. SEM images of CpEG nanofiller at different magnifications (see on the top) and AFM-3D and TEM images of T20BD + 1.8%CpEG sample (see on the bottom from left to right, respectively).

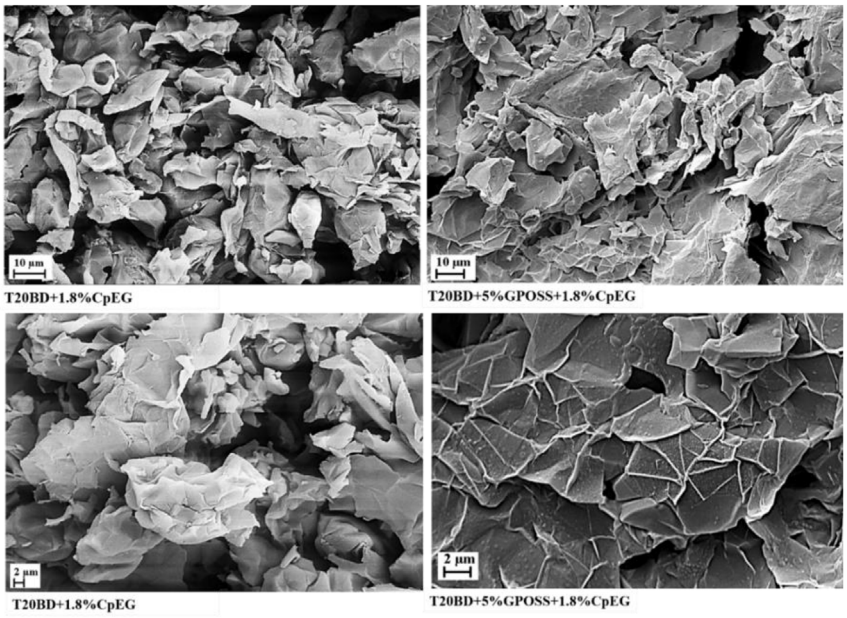

Fig. 10. SEM images at different magnifications of the fracture surface of the two epoxy-based composites filled with 1.8 wt% loading of CpEG with GPOSS and in absence of GPOSS.

reported in a recent published paper [47]. Concerning this last point, it has been observed by DMA of the same epoxy formulations containing GPOSS, that the inclusion of MWCNTs in the formulation containing GPOSS determines a phase with a lower transition in the mechanical spectrum (centred at about 210 °C) indicating the presence of a phase with greater mobility of chain segments. MWCNT are responsible for forming in the resin a second phase characterized by different cross-linking density. For the formulation T20BD + 5%GPOSS + 1.8%CpEG the Loss factor (tanδ) (see Fig. 8) shows a lower transition at about 120 °C (between 60 °C and 140 °C) confiming the presence of a phase at higher mobility of the chains segments. Furthermore, also the main peak of the sample is lower than the sample T20BD with a more widening profile. Hence, the formulation containing GPOSS is characterized by higher mobility and improved ability to react and adhere to the graphene layers. The chemical anchoring mechanisms are more effective due to the higher mobility of the polymeric matrix; this results in a better nanofiller dispersion as observed in Fig. 10 related to the SEM image of the sample T20BD + 5%GPOSS + 1.8%CpEG.

Figs. 11 and 12 show the TUNA-AFM micrographs and the corresponding 3D profiles of the T20BD + 1.8%CpEG and T20BD + 5%GPOSS + 1.8%CpEG epoxy formulations, respectively. The TUNA-AFM images were collected on etched samples to partially remove the resin surrounding the graphene sheets and to better observe the distribution of the nanofiller inside the epoxy matrix. For each sample, 4 TUNA-AFM image types which are the most common in contact mode, namely height (or topography) image, deflection error image, friction image, and tuna current image, are displayed below. The height image is the type of image most commonly reported and published. Usually, the height image is a map of differently coloured pixels, with a colour bar relating the colour to the height. This type of acquisition is really very useful as it allows to estimate both lateral (xy) and height (z) measurements. However, one reason other types of image are here shown is that such “height maps” do not always really “look like” the object in question, in other words, the appearance of a certain shape can be very different to that it would have in optical (or electron microscopy). What this means, is that, to the casual observer, such images do not display easily the shape of the features. Ways around this include shading the image, and more commonly, creating a pseudo-3D image from the height data. Because the deflection error image is equivalent to a map of the slope of the sample, it often displays the shape of the sample more easily. But it is worth noting that the z-scale in deflection is completely meaningless in terms of the sample structure. All it shows is how the tip deflected as it encountered sample topography. It is important to remember too that the best images are obtained when the deflection signals are minimised. The Friction, or Lateral Force images, are a map of lateral bending of the cantilever in contact mode. In other words, how the cantilever twists as it scans across the sample. This signal can be related to friction between the sample and the tip, but it also contains topographic contributions on a non-flat sample. In general, TUNA-AFM is most suited for the characterization of graphene nanoparticles due to its high spatial resolution and the various modes that allow probing different physical properties by simultaneously mapping the topography and current distribution at nanoscale level so that the direct correlation of a sample location with its electrical properties is easily possible. In fact, the 4 TUNA-AFM images reported below clearly show the morphological characteristics of the two samples and provide complementary information that helps the reader to a more complete understanding of the observed electrical properties. In the TUNA-AFM images of the two samples, crumpled morphology of the few layers of graphene with wrinkled and disordered sheet-like structure can be clearly observed, especially in 2D and 3D tuna current images. In fact, several graphene flakes appear homogeneously distributed across the sample surface. The flakes which are multilayered graphene sheets appear as flat areas. Higher structures at the edges are due to wrinkles and folds. The flakes are clearly observable for both samples in almost any image but they are most resolved in the tuna current images that have been recorded at the same time as the height, deflection error, friction images. The tuna current images show an increased contrast in the morphological features of graphene nanoplatelets. A clear correlation between the topography and the regions of high current was found whenever a measurable current can be recorded. The conductive measurements were carried out on the graphene based epoxy formulations because one the interesting properties of graphite-based materials is the high conductivity due to the delocalized electrons in between layers. In the case of the TUNA current image obtained at a bias voltage within a range of 1–2 V, conducting CpEG nanoparticles appear very bright, thus demonstrating their high conductivity and domains with lower conductivity values appear darker. As can be seen in the current profile, domains with different brightnesses present differences in the current value. A careful observation of the current profile of the T20BD + 1.8%CpEG (see Fig. 11) and T20BD + 5%GPOSS + 1.8%CpEG (see Fig. 12) epoxy resins allows to confirm that both samples are intrinsically conductive. In fact, for the sample T20BD + 1.8%CpEG, currents ranging from 1.4 to 2.7 pA were detected while

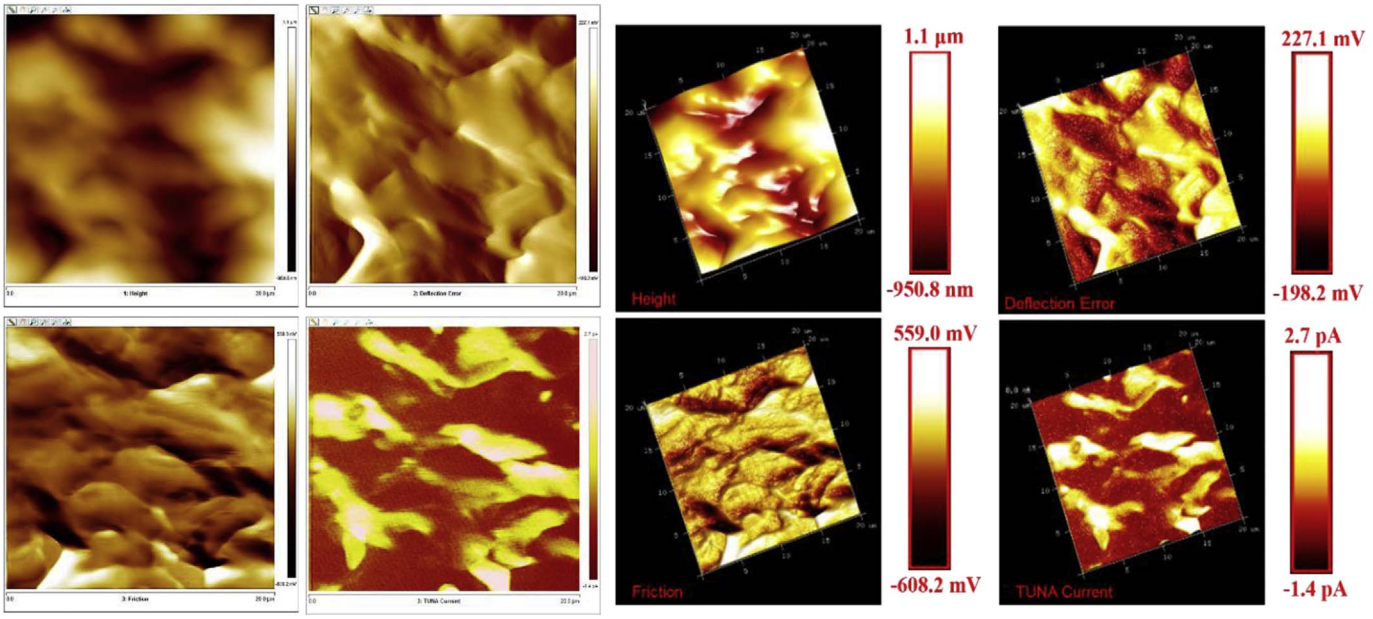

Fig. 11. TUNA-AFM micrographs (20 µm × 20 µm) of the fracture surface of the T20BD + 1.8%CpEG sample (see the 4 images from left to right on the left side: height, deflection error, friction and tuna current images) and the corresponding 3D profile (see the 4 images from left to right on the right side: height, deflection error, friction and tuna current images).

the sample T20BD + 5%GPOSS + 1.8%CpEG has shown currents ranging from 718.2 fA to 3.5 pA.

Hence, for the multifunctional nanocomposite T20BD + 5%GPOSS + 1.8%CpEG, the possibility to detect much lower currents (ranging from fA to pA) than those shown by the T20BD + 1.8% CpEG sample (of the pA order) confirms that the multifunctional nanocomposite exhibits greater electrical conductivity. In the multifunctional sample, most likely, the presence of the GPOSS flame retardant, also acting as a viscosity modulator, thus decreasing the resin viscosity [47] allows a more efficient dispersion of the CpEG nanofiller and, consequently, more effective conductive paths. In this regard, in Fig. 13 showing a comparison between the conductive paths of the two investigated epoxy nanocomposites, the evidence in both samples of the current proves that the CpEG nanoparticles are conductive as it is highlighted by the strong contrast of the colors in the tuna current micrographs. In particular, we can see that, although conductive nanofiller dispersion in the epoxy matrix is effective in both formulations, however, the multifunctional sample T20BD + 5%GPOSS + 1.8%CpEG show CpEG nanosheets with the high current flow located mainly at the edges ensuring a good transfer of electrical properties to the polymeric surface through a conductive network at nanoscale level.

As discussed before, for polymeric systems containing embedded electrical conductive carbon nanostructured forms (graphene-based nanoparticles, multi-wall carbon nanotubes, carbon nanofibres and nanowires etc.) [89], the TUNA-AFM investigation provides a map of nanofiller distribution at nanoscale level. This type of investigation can

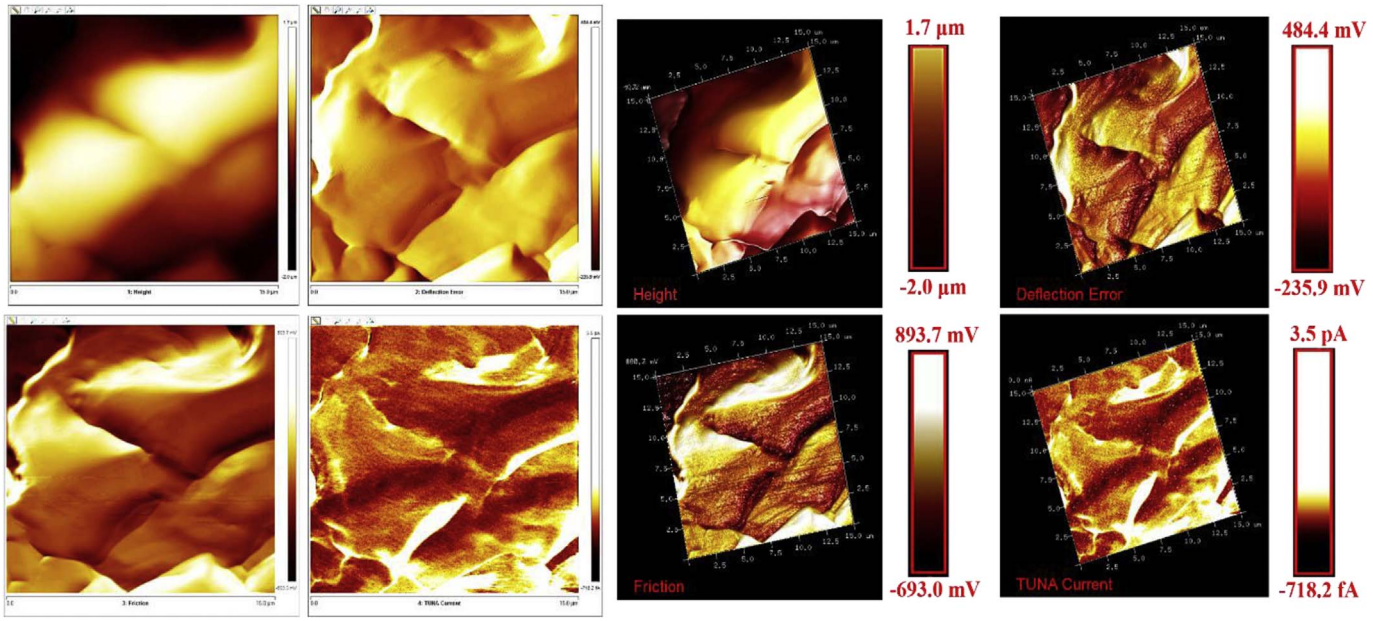

Fig. 12. TUNA-AFM micrographs (15 µm × 15 µm) of the fracture surface of the T20BD + 5%GPOSS + 1.8%CpEG sample (see the 4 images from left to right on the left side: height, deflection error, friction and tuna current images) and the corresponding 3D profile (see the 4 images from left to right on the right side: height, deflection error, friction and tuna current images).

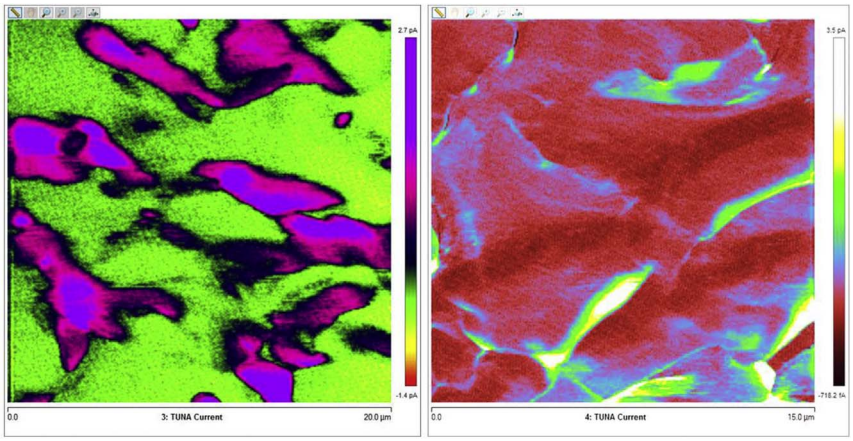

Fig. 13. TUNA-AFM micrograph (20 μm × 20 μm) of the fracture surface of the T20BD + 1.8%CpEG sample (see tuna current image on the left) and TUNA-AFM micrograph (15 μm × 15 μm) of the fracture surface of the T20BD + 5%GPOSS + 1.8%CpEG sample (see tuna current image on the right) respectively.

be extensively applied to evaluate and predict the influence of the nanofiller-matrix interactions not only on the local electrical conductivity, but also on many other properties of the nanocomposites depending on the extent of the interactions in the polymeric matrix. As an instance, it has been found that the carbon nanofillers uniformly dispersed in the polymeric matrix are able to strongly enhance material durability [90,91]. This technique also provides a powerful means to predict if the level of nanofiller dispersion is effectively to guarantee a good photo-oxidative stability of the designed nanocomposites.

4. Conclusion

TUNA-AFM technology was successfully applied to study the quantitative electrical characterization of the graphene based multifunctional nanocomposites. Hybrid nanocomposite seems to respond to applied bias voltages by giving a very effective conductive network at nanoscale level. The use of TUNA technology is an innovative tool for correlating the electrical properties of the designed structural material with its topographic features and for identifying and characterizing conductive pathways in graphene based polymer composites, without undergoing any prior treatment with silver paint that is usually used to create electrical contacts to the ground. This undoubtedly proves that the investigated samples are intrinsically conductive thus confirming conductive properties of the graphene nanoparticles in designed multifunctional advanced materials for aircraft lightning strike protection. In conclusion, the increase of LOI value and the decrease of the PHRR value, observed when GPOSS is used, and the increase of the time of ignition due to the inclusion of CpEG in epoxy systems together with the high electrical and mechanical properties ascribed to self-assembly mechanisms determined by attractive interactions between edge-carboxylated graphene particles and good thermostability imparted by CpEG nanofiller, confirm the successful obtainment of a multifunctional system meeting the process requirements that make the formulation suitable for structural applications in the aeronautical field.

Acknowledgements

The research leading to these results has received funding from the European Union's Seventh Framework Programme for research, technological development and demonstration under Grant Agreement N° 313978.

References

[1] He F, Mensitieri G, Lavorgna M, de Luna MS, Filippone G, Xia H, et al. Tailoring gas permeation and dielectric properties of bromobutyl rubber – graphene oxide nanocomposites by inducing an ordered nanofiller microstructure. Compos B Eng 2017;116:361–8https://doi.org/10.1016/j.compositesb.2016.10.076.

[2] Yan N, Buonocore G, Lavorgna M, Kaciulis S, Balijepalli SK, Zhan Y, et al. The role of reduced graphene oxide on chemical, mechanical and barrier properties of natural rubber composites. Compos Sci Technol 2014;102(1):74–81https://doi.org/10.1016/j.compscitech.2014.07.021.

[3] Scherillo G, Lavorgna M, Buonocore GG, Zhan YH, Xia HS, Mensitieri G, et al. Tailoring assembly of reduced graphene oxide nanosheets to control gas barrier properties of natural rubber nanocomposites. ACS Appl Mater Interfaces 2014;6(4):2230–4. http://dx.doi.org/10.1021/am405768m.

[4] Esposito Corcione C, Freuli F, Frigione M. Epoxy/expanded graphite stacks nanocomposites for cold-cured adhesives. J Adhes Sci Technol 2017;31(7):713–25https://doi.org/10.1080/01694243.2016.1230437.

[5] Shen MY, Chang TY, Hsieh TH, Li YL, Chiang CL, Hsiharng Y, et al. Mechanical properties and tensile fatigue of graphene nanoplatelets reinforced polymer nanocomposites. J Nanomater 2013;2013:9. 565401 https://doi.org/10.1155/2013/565401.

[6] Aoki HS, Dresselhaus M, editors. Physics of graphene, NanoScience and technology. Springer International Publishing Switzerland; 2014. XII, 350 pp., 145 illus., 66 illus. in color., Hardcover, ISBN:978-3-319-02632-9 http://www.springer.com/978-3-319-02632-9.

[7] Jagannadham K. Electrical conductivity of copper–graphene composite films synthesized by electrochemical deposition with exfoliated graphene platelets. J Vac Sci Technol B 2012;30(3):9. 03D109 https://doi.org/10.1116/1.3701701.

[8] Novoselov KS, Fal'ko VI, Colombo L, Gellert PR, Schwab MG, Kim K. A roadmap for graphene. Nature 2012;490:192–200. http://dx.doi.org/10.1038/nature11458.

[9] Zakaria MR, Abdul Kudus MH, Akil H Md, Mohd Thirmizir MZ. Comparative study of graphene nanoparticle and multiwall carbon nanotube filled epoxy nanocomposites based on mechanical, thermal and dielectric properties. Compos B Eng 2017;119:57–66. http://dx.doi.org/10.1016/j.compositesb.2017.03.023.

[10] Baur J, Silverman E. Challenges and opportunities in multifunctional nanocomposite structures for aerospace applications. MRS Bull 2007;32(4):328–34https://doi.org/10.1557/mrs2007.231.

[11] Salonitis K, Pandremenos J, Paralikas J, Chryssolouris G. Multifunctional materials: engineering applications and processing challenges. Int J Adv Manuf Technol 2010;49(5–8):803–26. http://dx.doi.org/10.1007/s00170-009-2428-6.

[12] Wei J, Vo T, Inam F. Epoxy/graphene nanocomposites–processing and properties: a review. RSC Adv 2015;5(90):73510–24. http://dx.doi.org/10.1039/C5RA13897C.

[13] Huang X, Qi X, Boey F, Zhang H. Graphene-based composites. Chem Soc Rev 2012;41(2):666–86. http://dx.doi.org/10.1039/C1CS15078B.

[14] Ye S, Feng J, Wu P. Highly elastic graphene oxide–epoxy composite aerogels via simple freeze-drying and subsequent routine curing. J Mater Chem A 2013;1(10):3495–502. http://dx.doi.org/10.1039/C2TA01142E.

[15] Heo Y, Im H, Kim J, Kim J. The influence of $Al(OH)_3$-coated graphene oxide on improved thermal conductivity and maintained electrical resistivity of Al_2O_3/epoxy composites. J Nanoparticle Res 2012;14(1196):10https://doi.org/10.1007/s11051-012-1196-7.

[16] Wang X, Xing W, Feng X, Yu B, Lu H, Song L, et al. The effect of metal oxide decorated graphene hybrids on the improved thermal stability and the reduced smoke toxicity in epoxy resins. Chem Eng J 2014;250:214–21https://doi.org/10.1016/j.cej.2014.01.106.

[17] An JE, Jeong YG. Structure and electric heating performance of graphene/epoxy composite films. Eur Polym J 2013;49(6):1322–30https://doi.org/10.1016/j.eurpolymj.2013.02.005.

[18] Ioniță M, Vlăsceanu GM, Watzlawek AA, Voicu SI, Burns JS, Iovu H. Graphene and functionalized graphene: extraordinary prospects for nanobiocomposite materials. Compos B Eng 2017;121:34–57. http://dx.doi.org/10.1016/j.compositesb.2017.03.031.

[19] Liu S, Chevali VS, Xu Z, Hui D, Wang H. A review of extending performance of epoxy resins using carbon nanomaterials. Compos B Eng 2018;136:197–214https://doi.org/10.1016/j.compositesb.2017.08.020.

[20] Hung P, Lau K, Fox B, Hameed N, Lee JH, Hui D. Surface modification of carbon fibre using graphene related materials for multifunctional composites. Compos B Eng 2018;133:240–57https://doi.org/10.1016/j.compositesb.2017.09.010.

[21] Li Y, Wang S, Wang Q, Xing M. A comparison study on mechanical properties of polymer composites reinforced by carbon nanotubes and graphene sheet. Compos B Eng 2018;133:35–41https://doi.org/10.1016/j.compositesb.2017.09.024.

[22] Kumar R, Singh R, Hui D, Feo L, Fraternali F. Graphene as biomedical sensing element: state of art review and potential engineering applications. Compos B Eng 2018;134:193–206https://doi.org/10.1016/j.compositesb.2017.09.049.

[23] Li Z, González AJ, Heeralal VB, Wang DY. Covalent assembly of MCM-41 nanospheres on graphene oxide for improving fire retardancy and mechanical property of epoxy resin. Compos B Eng 2018;138:101–12https://doi.org/10.1016/j.compositesb.2017.11.001.

[24] Guo W, Yu B, Yuan Y, Song L, Hu Y. In situ preparation of reduced graphene oxide/DOPO-based phosphonamidate hybrids towards high-performance epoxy nanocomposites. Compos B Eng 2017;123:154–64https://doi.org/10.1016/j.compositesb.2017.05.024.

[25] Frigione M, Lionetto F, Mascia L, Antonacci A. Novel epoxy-silica hybrid adhesives for concrete and structural materials: properties and durability issues. Adv Mater Res 2013;687:94–9. http://dx.doi.org/10.4028/www.scientific.net/AMR.687.94.

[26] Guadagno L, Naddeo C, Raimondo M, Vittoria V. Structural and morphological changes during UV irradiation of the trans-planar form of syndiotactic polypropylene. Polym Degrad Stabil 2008;93(1):176–87. http://dx.doi.org/10.1016/j.polymdegradstab.2007.10.003.

[27] Huang G, Chen S, Tang S, Gao J. A novel intumescent flame retardant functionalized graphene: nanocomposite synthesis, characterization, and flammability properties. Mater Chem Phys 2012;135:938–47https://doi.org/10.1016/j.matchemphys.2012.05.082.

[28] Raimondo M, Russo S, Guadagno L, Longo P, Chirico S, Mariconda A, et al. Effect of incorporation of POSS compounds and phosphorous hardeners on thermal and fire resistance of nanofilled aeronautic resins. RSC Adv 2015;5(15):10974–86https://doi.org/10.1039/C4RA11537F.

[29] Guadagno L, Longo P, Raimondo M, Naddeo C, Mariconda A, Vittoria V, et al. Use of Hoveyda-Grubbs' second generation catalyst in self-healing epoxy mixtures. Compos B Eng 2011;42(2):296–301https://doi.org/10.1016/j.compositesb.2010.10.011.

[30] Guadagno L, Raimondo M, Naddeo C, Longo P, Mariconda A, Binder WH. Healing efficiency and dynamic mechanical properties of self-healing epoxy systems. Smart Mater Struct 2014;23(4). 045001 https://doi.org/10.1088/0964-1726/23/4/045001.

[31] Raimondo M, Longo P, Mariconda A, Guadagno L. Healing agent for the activation of self-healing function at low temperature. Adv Compos Mater 2015;24(6):519–29https://doi.org/10.1080/09243046.2014.937135.

[32] Raimondo M, Guadagno L. Healing efficiency of epoxy-based materials for structural applications. Polym Compos 2013;34(9):1525–32https://doi.org/10.1002/pc.22539.

[33] Guadagno L, Raimondo M, Naddeo C, Longo P, Mariconda A. Self-healing materials for structural applications. Polym Eng Sci 2014;54(4):777–84https://doi.org/10.1002/pen.23621.

[34] Guadagno L, Mariconda A, Agovino A, Raimondo M, Longo P. Protection of graphene supported ROMP catalyst through polymeric globular shell in self-healing materials. Compos B Eng 2017;116:352–60https://doi.org/10.1016/j.compositesb.2016.10.075.

[35] Mariconda A, Longo P, Agovino A, Guadagno L, Sorrentino A, Raimondo M. Synthesis of ruthenium catalysts functionalized graphene oxide for self-healing applications. Polymer 2015;69:330–42https://doi.org/10.1016/j.polymer.2015.04.048.

[36] Guadagno L, Naddeo C, Raimondo M, Barra G, Vertuccio L, Russo S, et al. Influence of carbon nanoparticles/epoxy matrix interaction on mechanical, electrical and transport properties of structural advanced materials. Nanotechnology 2017;28(9):094001https://doi.org/10.1088/1361-6528/aa583d.

[37] Guadagno L, Raimondo M, Vertuccio L, Mauro M, Guerra G, Lafdi K, et al. Optimization of graphene-based materials outperforming host epoxy matrices. RSC Adv 2015;5(46):36969–78https://doi.org/10.1039/C5RA04558D.

[38] Vietri U, Guadagno L, Raimondo M, Vertuccio L, Lafdi K. Nanofilled epoxy adhesive for structural aeronautic materials. Compos B Eng 2014;61:73–83https://doi.org/10.1016/j.compositesb.2014.01.032.

[39] Guadagno L, Sarno M, Vietri U, Raimondo M, Cirillo C, Ciambelli P. Graphene-based structural adhesive to enhance adhesion performance. RSC Adv 2015;5(35):27874–86. http://dx.doi.org/10.1039/c5ra00819k.

[40] Guadagno L, Raimondo M, Vietri U, Vertuccio L, Barra G, De Vivo B, et al. Effective formulation and processing of nanofilled carbon fiber reinforced composites. RSC Adv 2015;5(8):6033–42https://doi.org/10.1039/C4RA12156B.

[41] Guadagno L, Vietri U, Raimondo M, Vertuccio L, Barra G, De Vivo B, et al. Correlation between electrical conductivity and manufacturing processes of nanofilled carbon fiber reinforced composites. Compos B Eng 2015;80:7–14https://doi.org/10.1016/j.compositesb.2015.05.025.

[42] Guadagno L, Raimondo M, Vittoria V, Vertuccio L, Naddeo C, Russo S, et al. Development of epoxy mixtures for application in aeronautics and aerospace. RSC Adv 2014;4(30):15474–88https://doi.org/10.1039/C3RA48031C.

[43] Guadagno L, Raimondo M, Longo P, Bonnaud L, Murariu O, Dubois Ph, et al. Multifunctional epoxy resin with enhanced flame resistance EUROPEAN PATENT APPLICATION EP2883896 (A1), Also published as: ITTO20131021 (A1) - Resina epossidica multifunzionale con accresciuta resistenza alla fiamma. 2015.

[44] Guadagno L, Raimondo M, Naddeo C, Russo S, Vittoria V, Russo S, et al. Dynamic mechanical properties of structural self-healing epoxy resins. Appl Mech Mater 2011;62:95–105https://doi.org/10.4028/www.scientific.net/AMM.62.95.

[45] Toldy A, Szolnoki B, Marosi G. Flame retardancy of fibre-reinforced epoxy resin composites for aerospace applications. Polym Degrad Stabil 2011;96(3):371–6https://doi.org/10.1016/j.polymdegradstab.2010.03.021.

[46] Gu H, Ma C, Gu J, Guo J, Yan X, Huang J, et al. An overview of multifunctional epoxy nanocomposites. J Mater Chem C 2016;4(25):5890–906. http://dx.doi.org/10.1039/C6TC01210H.

[47] Guadagno L, Naddeo C, Raimondo M, Barra G, Vertuccio L, Sorrentino A, et al. Development of self-healing multifunctional materials. Compos B Eng 2017;128:30–8https://doi.org/10.1016/j.compositesb.2017.07.003.

[48] Frigione M, Maffezzoli A, Finocchiaro P, Failla S. Cure kinetics and properties of epoxy resins containing a phosphorous-based flame retardant. Adv Polym Technol 2003;22(4):329–42. http://dx.doi.org/10.1002/adv.10060.

[49] Oliwa R, Heneczkowski M, Oleksy M, Galina H. Epoxy composites of reduced flammability. Compos B Eng 2016;95:1–8https://doi.org/10.1016/j.compositesb.2016.03.074.

[50] Kuo SW, Chang FC. POSS related polymer nanocomposites. Prog Polym Sci 2011;36(12):1649–96https://doi.org/10.1016/j.progpolymsci.2011.05.002.

[51] Cordes DB, Lickiss PD, Rataboul F. Recent developments in the chemistry of cubic polyhedral oligosilsesquioxanes. Chem Rev 2010;110(4):2081–173. http://dx.doi.org/10.1021/cr900201r.

[52] Shea KJ, Loy DA. Bridged polysilsesquioxanes. Molecular-engineered hybrid Organic−Inorganic materials. Chem Mater 2001;13(10):3306–19. http://dx.doi.org/10.1021/cm011074s.

[53] Lickiss PD, Rataboul F. Chapter 1-Fully Condensed polyhedral oligosilsesquioxanes (POSS): from synthesis to application. Hill A, Fink MJ, editors. Advances in organometallic chemistry 1st edition, vol. 57. San Diego, CA, USA: Elsevier Academic Press Inc; 2008. p. 1–116.

[54] Ayandele E, Sarkar B, Alexandridis P. Polyhedral oligomeric silsesquioxane (POSS)-Containing polymer nanocomposites. Nanomaterials 2012;2:445–75. http://dx.doi.org/10.3390/nano2040445.

[55] Harrison PG. Silicate cages: precursors to new materials. J Organomet Chem 1997;542(2):141–83https://doi.org/10.1016/S0022-328X(96)06821-0.

[56] Chemartin L, Lalande P, Peyrou B, Chazottes A, Elias PQ, Delalondre C, et al. Direct effects of lightning on aircraft structure: analysis of the thermal, electrical and mechanical constraints. J Aero Lab 2012;5:1–15.

[57] Gagné M, Therriau D. Lightning strike protection of composites. Prog Aero Sci 2014;64:1–16https://doi.org/10.1016/j.paerosci.2013.07.002.

[58] Hirano Y, Katsumata S, Iwahori Y, Todoroki A. Artificial lightning testing on graphite/epoxy composite laminate. Compos Part A Appl Sci Manuf 2010;41(10):1461–70https://doi.org/10.1016/j.compositesa.2010.06.008.

[59] Gou J, Tang Y, Liang F, Zhao Z, Firsich D, Fielding J. Carbon nanofiber paper for lightning strike protection of composite materials. Compos B Eng 2009;41(2):192–8https://doi.org/10.1016/j.compositesb.2009.06.009.

[60] Karch C, Metzner C. Lightning protection of carbon fibre reinforced plastics - an Overview. 33rd international conference on lightning protection, ICLP 2016, Estoril, Lisboa; Portugal 2016:7791441http://dx.doi.org/10.1109/ICLP.2016.7791441.

[61] Miraftab R, Karimi B, Bahlakeh G, Ramezanzadeh B. Complementary experimental and quantum mechanics approaches for exploring the mechanical characteristics of epoxy composites loaded with graphene oxide-polyaniline nanofibers. J Ind Eng Chem 2017;53:348–59https://doi.org/10.1016/j.jiec.2017.05.006.

[62] Romano V, Naddeo C, Vertuccio L, Lafdi K, Guadagno L. Experimental evaluation and modeling of thermal conductivity of tetrafunctional epoxy resin containing different carbon nanostructures. Polym Eng Sci 2017;57(7):779–86. http://dx.doi.org/10.1002/pen.24629.

[63] Rezek B, Stuchlık J, Fejfar A, Koc˘ka J. Microcrystalline silicon thin films studied by atomic force microscopy with electrical current detection. J Appl Phys 2002;92(1):587–93. http://dx.doi.org/10.1063/1.1486032.

[64] Richter S, Geva M, Garno JP, Kleiman RN. Metal–insulator–semiconductor tunneling microscope: two-dimensional dopant profiling of semiconductors with conducting atomic-force microscopy. Appl Phys Lett 2000;77(3):456–8. http://dx.doi.org/10.1063/1.127008.

[65] Xu D, Watt GD, Harb JN, Davis RC. Electrical conductivity of ferritin proteins by conductive AFM. Nano Lett 2005;5(4):571–7. http://dx.doi.org/10.1021/nl048218x.

[66] Musumeci C, Liscio A, Palermo V, Samori P. Electronic characterization of supramolecular materials at the nanoscale by conductive atomic force and kelvin probe force microscopies. Mater Today 2014;17(10):504–17https://doi.org/10.1016/j.mattod.2014.05.010.

[67] Prastani C, Vetushka A, Fejfar A, Nanu M, Nanu D, Rath JK, et al. Conductivity mapping of nanoparticles by torsional resonance tunneling atomic force microscopy. Appl Phys Lett 2012;101:4. 083107 https://doi.org/10.1063/1.4744601.

[68] Yanef V, Rommel M, Lemberger M, Petersen S, Amon B, Erbacher T, et al. Tunneling atomic-force microscopy as a highly sensitive mapping tool for the characterization of film morphology in thin high-k dielectrics. Appl Phys Lett 2008;92(25):3. 252910 https://doi.org/10.1063/1.2953068.

[69] Desbief S, Hergué N, Douhéret O, Surin M, Dubois P, Geerts Y, et al. Nanoscale investigation of the electrical properties in semiconductor polymer–carbon nanotube hybrid materials. Nanoscale 2012;4(8):2705–12. http://dx.doi.org/10.1039/C2NR11888B.

[70] Gutierrez J, Mondragon I, Tercjak A. Quantitative nanoelectrical and nanomechanical properties Of nanostructured hybrid composites by PeakForce tunneling atomic force microscopy. J Phys Chem C 2014;118(2):1206–12. http://dx.doi.org/10.1021/jp407690s.

[71] Palermo V, Liscio A, Palma M, Surin M, Lazzaroni R, Samorì P. Exploring nanoscale electrical and electronic properties of organic and polymeric functional materials by atomic force microscopy based approaches. Chem Commun 2007;32:3326–37. http://dx.doi.org/10.1039/b701015j.

[72] Samorì P. Scanning probe microscopies beyond imaging. J Mater Chem 2004;14(9):1353–66. http://dx.doi.org/10.1039/B314626J.
[73] Chung DDL. A review of exfoliated graphite. J Mater Sci 2016;51(1):554–68. http://dx.doi.org/10.1007/s10853-015-9284-6.
[74] Polymer Green Flame Retardants, 1st Edition, Editors: Papaspyrides C., Kiliaris P., eBook ISBN: 9780444538093, Hardcover ISBN: 9780444538086, Imprint: Elsevier, Published Date: 21st August 2014.
[75] Harniman RL, Fox Oliver JL, Janssen W, Drijkoningen S, Haenen K, May PW. Direct observation of electron emission from grain boundaries in CVD diamond by PeakForce-controlled tunnelling atomic force microscopy. Carbon 2015;94:386–95https://doi.org/10.1016/j.carbon.2015.06.082.
[76] Lanza M. Conductive atomic force microscopy. Berlin, Germany: Wiley-VCH; 2017. p. 400. ISBN 978-3-527-34091-0.
[77] Hourani W. Nanoscale characterization of leakage currents in ultra-thin oxide layers for microelectronics Other INSA de Lyon; 2011. English.
[78] Dickinson JC. AFM, CAFM, and EFM studies of the GaN system Theses and Dissertations Virginia Commonwealth University VCU Scholars Compass; 2003 Downloaded from http://scholarscompass.vcu.edu/etd/4522.
[79] Sang B, Li ZW, Li XH, Yu LG, Zhang Z. Graphene-based flame retardants: a review. J Mater Sci 2016;51(18):8271–95. http://dx.doi.org/10.1007/s10853-016-0124-0.
[80] De Vivo B, Lamberti P, Spinelli G, Tucci V, Guadagno L, Raimondo M, et al. Improvement of the electrical conductivity in multiphase epoxy-based MWCNT nanocomposites by means of an optimized clay content. Compos Sci Technol 2013;89:69–76. http://dx.doi.org/10.1016/j.compscitech.2013.09.021.
[81] Guadagno L, Raimondo M, Vittoria V, Vertuccio L, Lafdi K, De Vivo B, et al. The role of carbon nanofiber defects on the electrical and mechanical properties of CNF-based resins. Nanotechnology 2013;24(30):305704. http://dx.doi.org/10.1088/0957-4484/24/30/305704.
[82] De Vivo B, Guadagno L, Lamberti P, Raimondo M, Spinelli G, Tucci V, et al. Electrical properties of multi-walled carbon nanotube/tetrafunctional epoxy-amine composites. Am Inst Phys Conf Proc. 2012;1459(1):199–201. http://dx.doi.org/10.1063/1.4738442.
[83] Kandola BK, Horrocks AR, Myler P, Blair D. Thermal characterization of thermoset matrix resins. ACS Symposium Series Nelson GL, Wilkie CA, editors. Fire and polymers, vol. 797. Washington: ACS; 2001. p. 344–60. http://dx.doi.org/10.1021/bk-2001-0797.ch027 [Chapter 27].
[84] Kandola BK, Biswas B, Price D, Horrocks AR. Studies on the effect of different levels of toughener and flame retardants on thermal stability of epoxy resin. Polym Degrad Stabil 2010;95(2):144–52https://doi.org/10.1016/j.polymdegradstab.2009.11.040.
[85] Liu YL, Hsiue GH, Lan CW, Chiu YS. Phosphorus-containing epoxy for flame retardance: IV. Kinetics and mechanism of thermal degradation. Polym Degrad Stabil 1997;56(3):291–9https://doi.org/10.1016/S0141-3910(96)00177-2.
[86] Gojny FH, Wichmann MHG, Fiedler B, Kinloch IA, Bauhofer W, Windle AH, et al. Evaluation and identification of electrical and thermal conduction mechanisms in carbon nanotube/epoxy composites. Polymer 2006;47(6):2036–45. http://dx.doi.org/10.1016/j.polymer.2006.01.029.
[87] Gallego MM, Verdejo R, Khajet M, Ortiz de Zarate JM, Essalhi M, Lopez-Manchado MA. Thermal conductivity of carbon nanotubes and graphene in epoxy nanofluids and nanocomposites. Nanoscale Res Lett 2011;6(1):7. 610 http://www.nanoscalereslett.com/content/6/1/610.
[88] Chen J. Nanostructuration of epoxy networks by using polyhedral oligomeric silsesquioxanes POSS and its copolymers Other INSA de Lyon; 2012.
[89] Vertuccio L, Guadagno L, Spinelli G, Russo S, Iannuzzo G. Effect of carbon nanotube and functionalized liquid rubber on mechanical and electrical properties of epoxy adhesives for aircraft structures. Compos B Eng 2017;129:1–10. http://dx.doi.org/10.1016/j.compositesb.2017.07.021.
[90] Guadagno L, Raimondo M, Naddeo C, Di Bartolomeo A, Lafdi K. Influence of multiwall carbon nanotubes on morphological and structural changes during UV irradiation of syndiotactic polypropylene films. J Polym Sci B Polym Phys 2012;50(14):963–75. http://dx.doi.org/10.1002/polb.23093.
[91] Guadagno L, Naddeo C, Raimondo M, Gorrasi G, Vittoria V. Effect of carbon nanotubes on the photo-oxidative durability of syndiotactic polypropylene. Polym Degrad Stabil 2010;95(9):1614–26. http://dx.doi.org/10.1016/j.polymdegradstab.2010.05.030.